Copyright © 2008 Tech Science Press CMES, vol.25, no.3, pp.149-164, 2008

Dynamic Simulation of Carbon Nanotubes in Simple Shear Flow

Wenzhong Tang[1] **and Suresh G. Advani**[1]

Abstract: In this paper, a method for studying nanotube dynamics in simple shear flow was developed. A nanotube was described as a flexible fiber with a sphere-chain model. The forces on the nanotube were obtained by molecular dynamics simulations. The motion of the nanotube in simple shear flow was tracked by the flexible fiber dynamics method [Tang and Advani (2005)]. The viscosity of dilute nanotube suspensions was calculated based on the nanotube dynamics, and the effects of the aspect ratio and initial curvature of the nanotube on suspension viscosity are explored and discussed.

1 Introduction

It is well known that the properties of a fiber reinforced polymer composite are related to its microstructure including fiber distribution and orientation [Liakus et al. (2003), Kim et al. (2005)]. Fiber dynamics in suspension flow play an important role in determining the microstructure and properties of the resulting composite. Hence the dynamics of fibers in a flowing suspension has been of scientific and engineering interest for nearly one century [Jeffrey (1923), Taylor (1923), Trevelyan and Mason (1951), Bretherton (1962), Jeffery and Acrivos (1976), Vincent and Agassant (1985), Advani and Tucker (1990), Chiba and Nakamura (1998), Xu and Aidun (2005)]. Not unlike fiber reinforced polymer composites, the properties of polymer nanotube composites are also related to the distribution and orientation of carbon nanotubes in polymer matrices. While good dispersion of nanotubes can improve the mechanical properties of a polymer nanotube composites by 50-60% [Kumar et al. (2002)], the incorporation of nanotubes into a polymer may have no enhancement, or even show degradation in mechanical properties due to poor dispersion [Bhattacharyya et al. (2003)]. Alignment of nanotubes also has a significant effect on the electrical and mechanical properties of polymer nanotube composites. Du et al. (2005) studied a series of SWNT/PMMA (polymethyl methacrylate) composite fibers in which the degree of nanotube alignment was controlled by melt spinning conditions. They found that, at a fixed SWNT content, the electrical conductivity in the alignment direction increased sharply with increasing alignment. Thostenson and Chou (2002) fabricated polystyrene based composite films with highly aligned and randomly oriented carbon nanotubes. It was reported that the improvement in elastic modulus with the aligned nanotube composite was five times higher than the randomly oriented composite. Similar to fiber reinforced composites, the orientation and distribution of CNTs in a polymer matrix are determined by the flow of nanotube suspension. To understand how carbon nanotubes move during processing induced flow, there is a need to study nanotube dynamics in suspension flow.

In polymer nanocomposites processing, the mixing of carbon nanotubes in a fluid also alters its rheological properties. Kinloch et al. (2002) investigated the rheological behavior of oxidized nanotubes in water suspensions using a cone and plate rheometer. They found that, under steady shear, the suspensions exhibited shear thinning behavior. Fan and Advani (2007) characterized the viscosity of CNT/epoxy suspensions. They found that the CNT/epoxy suspensions exhibited a shear thinning behavior whereas the pure epoxy behaved like a Newtonian fluid. Other experimental studies have also exhibited the shear thinning behavior of nanotube suspensions [Abdel-Goad

[1] Department of Mechanical Engineering and Center for Composite materials, University of Delaware, Newark, DE 19716-3140, USA

and Pötschke (2005), Sung et al. (2006), Huang et al. (2006)]. Such experimental work suggests that nanotubes tend to align during shear reducing the viscosity as observed in case of high molecular weight polymers and fiber suspensions. However, there has not been much theoretical work that has been done to be able to describe the movement and orientation of carbon nanotubes during flow of such suspensions. To understand how carbon nanotubes change their configuration and behavior in a flowing nanotube suspension, there is a need to study nanotube dynamics in suspension flow.

Since the nanotube scale is much smaller than a micron, usually molecular dynamics simulations are used to investigate the interactions between a nanotube and its surrounding fluid molecules [Walther et al. (2004), Tang and Advani (2006, 2007)]. In such studies, a nanotube-fluid system is explored at a unit cell level by applying periodic boundary conditions, and the length of a nanotube is restricted to only an order of magnitude larger than its diameter. However, when a real nanotube with high aspect ratio (length-to-diameter ratio, Ar, usually over 100) in simple shear flow is considered, such a nanotube-fluid system would be too large for molecular dynamics simulation due to formidable number of calculations required. Although carbon nantoubes have a very large Young's modulus in the axial direction, they are highly flexible in the direction perpendicular to their axis [(Ajayan et al. (1994), Ruoff and Lorents (1995), Falvo et al. (1997), Ajayan and Zhou (2001), Dalmas et al. (2006)]. In this paper, we will view a long carbon nanotube as a flexible fiber and neglect its stiffness. The dynamics of a carbon nanotube in simple shear water flow will be investigated by coupling the flexible fiber dynamics [Tang and Advani (2005)] with forces on the nanotube obtained by molecular dynamics simulation. We use water instead of a polymer resin as our suspending fluid because the calculations required to obtain the drag forces by MD simulation with polymer molecules are formidable, which may take months or even years using current computation resources. However, the Reynolds number is in the creeping regime which does eliminate the influence of inertia as one would expect in polymer flows. Based on the nanotube dynamics, we will also calculate the viscosity of nanotube suspensions and investigate the effect of nanotube aspect ratio and initial configuration on suspension viscosity.

2 Flexible fiber dynamics

In fiber composites manufacturing, considerable benefit can be gained by increasing the fiber length. A longer fiber with a larger aspect ratio can significantly improve the composite strength than its short fiber counterpart [McClelland and Gibson (1990), Bartus and Vaidya (2005)]. When the aspect ratio of a fiber increases, it becomes more flexible. The dynamics of flexible fibers in a flowing suspension has been of engineering and scientific interest for three decades [Hinch (1976), Yamamoto and Matsuoka (1993, 1994), Ross and Klingenberg (1997), Joung et al. (2001), Tornberg and Shelley (2004)]. In our previous work [Tang and Advani (2005)], we employed an optimization method and a Sphere-Chain fiber model to investigate flexible fiber dynamics in simple shear flow. To simulate the motion of a long flexible fiber in flow, the fiber was modeled as a chain of spheres (Figure 1). In the model, a continuous fiber of length L_f and diameter d_f was discretized into a number of small segments of length L_0; next the segments were lumped into individual spheres, its mass m_s being the same as that of the corresponding segments; finally the spheres were connected by rigid massless rods of length L_0 to maintain constant fiber length, and ball-socket joints were used to allow free rotation between neighboring segments. With the trajectory of the spheres, this Sphere-Chain model was used to describe the motion of a flexible fiber in suspension flows.

To track the motion of a flexible fiber in shear flow, the positions of the spheres were determined by the forces acting on them. The spheres are subjected to two types of forces: external forces by the flowing fluid and internal forces by the neighboring spheres through the rigid massless rods. External forces on the spheres were calculated from the cross and axial drag forces on their cor-

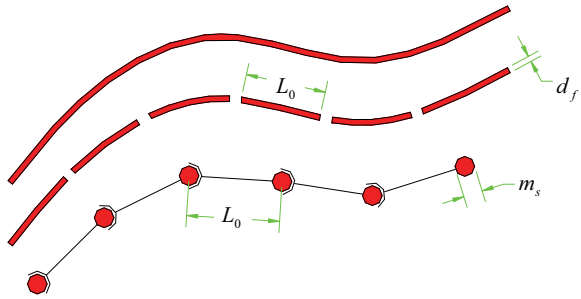

Figure 1: Sphere-Chain model of a flexible fiber

responding fiber segments. Figure 2 illustrates the drag force and its components on a fiber segment.

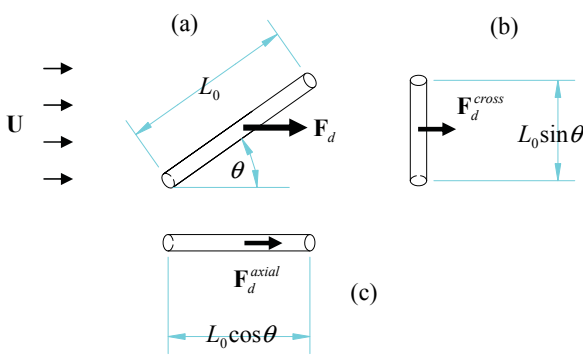

Figure 2: Drag force on a fiber segment: (a) total drag, (b) cross drag, and (c) axial drag

The angle between the directions of the fiber segment and the flow is θ $(0 \le \theta \le \frac{\pi}{2})$. The total drag force $\mathbf{F}_d$ can be calculated as

$$F_d = (L_0 \sin\theta) F_d^{cross} + (L_0 \cos\theta) F_d^{axial}, \tag{1}$$

where $L_0 \cos\theta$ and $L_0 \sin\theta$ are the projected lengths of the fiber segment in the flow and transverse directions respectively, and F_d^{cross} and F_d^{axial} are cross and axial drag per unit length respectively.

Figure 3 illustrates our approach to advance the fiber motion from one time step to the next time step. Figure 3a shows, at the current time step, a fiber consisting of spheres at different positions $\mathbf{R}_i^t$, velocities $\mathbf{V}_i^t$, and external forces $\mathbf{F}_i^t$ $(i = 1, 2, \cdots, n)$. To obtain the new position of the fiber at the next time step, first the constraints between neighboring spheres are removed (Figure 3b), enabling each sphere to move independently, which leads to a set of pseudo new sphere positions $\overline{\mathbf{R}}_i^{t+1}$ (Figure 3c). Let $\mathbf{R}_i^{t+1}$ be the actual new positions of the spheres (Figure 3d). Intuitively the actual new positions $\mathbf{R}_i^{t+1}$ of a fiber can be derived from the pseudo new positions $\overline{\mathbf{R}}_i^{t+1}$. Let $d_i = \left|\mathbf{R}_i^{t+1} - \overline{\mathbf{R}}_i^{t+1}\right|$ be the distance between the pseudo and the actual new positions of the ith sphere in the fiber. Inspired by the minimal principles [Marion (1970)], we seek the actual new positions by minimizing the sum of square of d_i, that is,

$$\min \sum_{i=1}^{n} d_i^2. \tag{2}$$

Since the fiber is assumed to be inextensible, the constraints are expressed as

$$\left|\mathbf{R}_{i+1}^{t+1} - \mathbf{R}_i^{t+1}\right| = L_0,\ i = 1, 2, \cdots, n-1 \tag{3}$$

where L_0 is the length of each segment. Therefore, the mathematical model is in principle a typical optimization problem. This optimization method was verified by particle dynamics [Tang and Advani (2005)].

Based on fiber dynamics, the viscosity of a fiber suspension in shear flow can be calculated from its effective stress tensor. The bulk stress $\langle \tau_{mn} \rangle$ in the suspension is defined by Batchelor's effective stress tensor as [Batchelor (1970); Ross and Klingenberg (1997)]

$$\langle \tau_{mn} \rangle = \tau_{mn}^{\infty} + \frac{1}{V} \int_{V_0} \tau_{mn} dV_0 = \tau_{mn}^{\infty} + \frac{V_f}{V_0} \int_{V_0} \tau_{mn} dV_0 \tag{4}$$

where τ_{mn}^{∞} is the stress tensor that would exist in the absence of the fiber; V is the volume of the periodic unit cell; V_0 is the volume of the fiber; $V_f = V_0/V$ is the volume fraction of the fiber in the unit cell, and τ_{mn} is the stress tensor on the fiber with shear stress component τ_{xy} calculated as [Timoshenko and Goodier (1970)]

$$\tau_{xy} = \sigma \sin\alpha \cos\alpha = \frac{4 f_{i,i+1}}{\pi d_f^2} \sin\alpha \cos\alpha \tag{5}$$

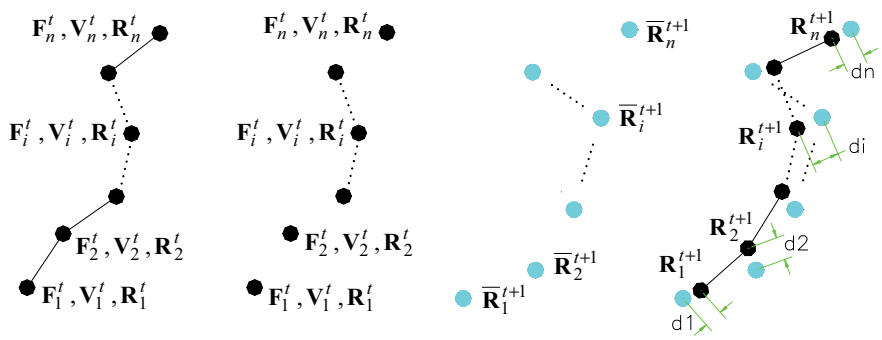

Figure 3: Mathematical model for advancing fiber motion: (a) current position; (b) uncoupled spheres; (c) pseudo new position; and (d) actual new position

where σ is the normal stress in the fiber axis direction, $f_{i,i+1}$ is the internal force in the fiber segment between i^{th} and $(i+1)^{th}$ spheres which can be obtained from fiber dynamics [details in Tang and Advani (2005)], α $(0 \leq \alpha < 2\pi)$ is the angle between the axis of the fiber segment and the x axis (Figure 4), and d_f is the diameter of the fiber. The bulk viscosity of the suspension is defined as

$$\mu_{bulk} = \langle \tau_{xy} \rangle / \dot{\gamma}_{xy}. \tag{6}$$

where $\dot{\gamma}_{xy}$ is the shear rate in the suspension. Then the relative viscosity of the suspension with respect to the fluid viscosity is calculated as

$$\mu_r = \mu_{bulk}/\mu. \tag{7}$$

Details of flexible fiber dynamics can also be found in Tang and Advani (2005), in which the verification of the model was presented.

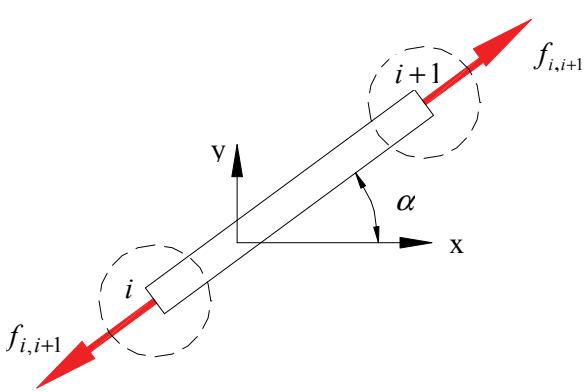

Figure 4: Internal force contributing to the shear stress component in the fiber

3 Molecular dynamics simulation

3.1 Drag forces acting on a nanotube

In this work, we consider zigzag (6, 0) nanotubes with a diameter of $d = 0.4752\,nm$ and an aspect ratio $Ar = 50 - 400$. To simulate the motion of high aspect ratio nanotube in simple shear flow with water as the suspending fluid, the nanotube is described using the Sphere-Chain flexible fiber model (Figure 1). When the dynamics of a flexible fiber in simple shear flow were investigated, the forces (axial and cross drag) acting on a fiber by its suspending fluid, were computed using equations formulated using continuum mechanics [Hinch (1976), Tang and Advani (2005)]. However, our molecular dynamics simulations on nanotube in both liquid argon and water flows have shown that the drag and drag coefficient on a nanotube are different from those calculated using continuum mechanics methods [Tang and Advani (2006, 2007)]. In the flow speed range of engineering applications, the cross drag coefficient from MD simulation is larger than the ones calculated from continuum mechanics equations. The difference in drag coefficient increases as the flow speed decreases. On the other hand, the axial drag on a nanotube from MD simulations was very small when compared to the calculation from continuum mechanics. Therefore, when studying the dynamics of a nanotube in simple shear flow, the cross and axial drag forces on the nanotube will be obtained by MD simulations. Since the axial force acting on the end of a nanotube might be large compared with the axial drag on

nanotube surface, this end force will also be considered. Figure 2 illustrated the total drag force and its components on a segment of a fiber but this could be for a tube segment. If the angle between the tube segment and the flow direction is θ, the total force acting on the tube segment is calculated as

$$F_d = (L_0 \sin\theta) F_d^{cross} + (L_0 \cos\theta) F_d^{axial} + (\delta \cos\theta) F_{end}. \quad (8)$$

This equation is similar to Equation (1) for a fiber segment except that the end force is included for the nanotube. Here, F_{end} is the end force when $\theta = 0$; δ is 1 for the two segments at the two ends of the tube and 0 for all other segments.

3.2 Potentials, units and time steps in MD simulation

In this study, molecular dynamics simulations of a zigzag (6, 0) nanotube ($d = 0.475\,nm$) in water flow were performed to obtain the drag forces. In simulation, the nanotube is surrounded by water molecules at 25 $°C$, with a density of ρ =996 kg/m^3 and a dynamic viscosity of μ =8.90×10^{-4} $kg/m \cdot s$ [Kundu (1990)]. The water molecule was described with the extended simple point charge (SPC/E) model [Berendsen et al. (1987), Kusalik and Svishchev (1994)]. In this model, the bond length ($r_{OH} = 1 \times 10^{-10}\,m$) and the bond angle ($\angle HOH = 109.47°$) are fixed; the oxygen carries a negative electric charge of $q_O = -0.8476e$ and each hydrogen atom carries a positive charge of $q_H = 0.4238e$; and the oxygen-oxygen well depth and van der Waals radius are $\varepsilon_{OO} = 0.6501\,KJ/mol$ and $\sigma_{OO} = 3.166 \times 10^{-10} m$ respectively. The interactions between two water molecules consist of a Lennard-Jones potential between the oxygen atoms and a Coulomb potential comprising of all electrically interactive pairs. The Leonard-Jones potential between the oxygen pair is calculated as [Kotsalis et al. (2004)]

$$E_{LJ}(r_{OO}) = 4\,\varepsilon_{OO} \left[\left(\frac{\sigma_{OO}}{r_{OO}} \right)^{12} - \left(\frac{\sigma_{OO}}{r_{OO}} \right)^{6} \right], \quad r_{OO} \le r_{c_LJ} \quad (9)$$

where r_{OO} is the distance between the two oxygen atoms and $r_{c_LJ} = 1.0 \times 10^{-9} m$ is a cutoff distance beyond which the Lennard-Jones interaction is so small that it can be neglected. The Coulomb potential between two electrically interactive sites is expressed as [Kotsalis et al. (2004)]

$$E_{El}(r_{ij}) = \frac{q_i q_j}{4\pi\,\varepsilon_0 r_{ij}}, \quad r_{ij} \le r_{c_EL} \quad (10)$$

where q_i and q_j are the electric charges of the two sites, $\varepsilon_0 = 8.854 \times 10^{-12} F/m$ is the permittivity in vacuum, r_{ij} is the distance between the two interaction sites, and r_{c_EL} is a cutoff distance beyond which the electrostatic interaction is neglected. The truncation of the Coulomb potential has been shown to have little effect on the thermodynamic and structural properties of water for cutoff distances larger than $6.0 \times 10^{-10} m$ [Andrea et al. (1984)]. In this work, we employed a cutoff distance of $r_{c_EL} = 1.14 \times 10^{-9} m$. A larger value did not make much difference in the value of the calculated drag force on the nanotube from our simulation. As in our previous work [Tang and Advani (2006)] and in the work by Gordillo and Marti (2003) and by Walther et al. (2004), the carbon nanotube was modeled as a rigid structure, in which the bonds between carbon atoms are fixed (bond length $r_{C-C} = 1.42 \times 10^{-10} m$) and the carbon atoms do not move relative to each other. The rigid tube model is used in our study since it has been verified that the consideration of carbon mobility has little effect on the hydrodynamic properties of water/carbon nanotube system [Werder et al. (2003)]. The nanotube-water interaction is described by the Lennard-Jones potential between the carbon and oxygen sites which is expressed as

$$E_{LJ}(r_{CO}) = 4\,\varepsilon_{CO} \left[\left(\frac{\sigma_{CO}}{r_{CO}} \right)^{12} - \left(\frac{\sigma_{CO}}{r_{CO}} \right)^{6} \right], \quad r_{CO} \le r_{c_LJ} \quad (11)$$

where $\varepsilon_{CO} = 0.4389\,KJ/mol$ and $\sigma_{CO} = 3.19 \times 10^{-10} m$ are the carbon-oxygen well depth and carbon-oxygen van der Waals radius respectively [Bojan and Steele (1987), Werder et al. (2003)], r_{CO} is the distance between the interaction sites,

and $r_{c_LJ} = 1.0 \times 10^{-9} m$ is the same cutoff distance as in Equation 9 for oxygen-oxygen pairs. With the above potentials, codes based on the one by Rapaport (1995) for two-dimensional liquid argon flow around a circular obstacle were developed to simulate water flow around a carbon nanotube. In our calculation, non-dimensional parameters are used by selecting σ_{OO} , ε_{OO} , m_{H_2O} (molecular weight of water), and q_H as the units of length, energy, mass and electric charge respectively [Rapaport (1995)]. The resulting reduced units are listed in Table 1. In this paper, parameters will be expressed

in non-dimensional units unless otherwise stated. In literature, a time step as large as $2\times10^{-15} s$ has been used for water-nanotube systems [DiLeo and Maranon (2003), Kalra et al. (2003), Werder et al. (2003)]. In our study, the equations of motion were integrated with predictor-corrector method [Rapaport (1995)] and a time step $\Delta t = 6.25 \times 10^{-16} s$ (0.000375 in reduced units) was adopted. A smaller step did not change the value of the calculated drag.

3.3 Cross drag

To obtain the cross drag on a nanotube in water flow, water molecules flowing across a single walled zigzag (6, 0) nanotube was simulated. Figure 5 illustrates a unit cell of a nanotube-water system. In the $L \times W \times H$ ($13.26 \times 13.26 \times 0.85 nm^3$) cubic cell, the nanotube is fixed at the center of the system, with its axis along the z direction. Initially, the water molecules were evenly placed in

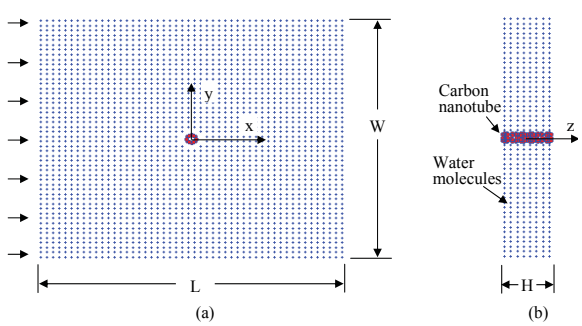

Figure 5: Unit cell of a nanotube-water system: (a) top view; (b) side view

the domain with random orientations. All water molecules had identical translational and rotational speeds but move in random directions resulting in a system with zero resultant velocity. The cross flow was initialized by superimposing a desired flow velocity **U** in the x direction on all water molecules, and maintaining it by first redefining random velocity of molecules within $0.025 \times L$ of the $x = \pm L/2$ boundaries every 40 time steps, and then superimposing the desired flow velocity **U** on these molecules. This technique of maintaining uniform flow removes excess heat, which is equivalent to adding a heat sink at the inlet [Rapaport (1995)]. Periodic boundary conditions were applied in all three directions - when a molecule passes through one face of the unit cell, it reappears on the opposite face with the same velocity. At each time step, the drag force on the nanotube (instantaneous drag) was obtained by summing up forces on all carbon atoms. To characterize the drag on the nanotube, converged time-averaged value was obtained by averaging the instantaneous drag over time, on a domain size of $L \times W \times H = 13.26 \times 13.26 \times 0.85 nm^3$, which contained 48 carbon atoms and 4976 water molecules. A larger domain does not make much difference in the value of the calculated drag. The number of time steps needed for a run varied from 800,000 to 1,600,000, depending on the magnitude of the flow velocity **U**. Generally, a smaller flow speed requires more time step to yield converged drag. The details about how to obtain the converged time-averaged drag can be found elsewhere [Tang and Advani (2007)], in which the drag and drag coefficient from MD simulation were compared with the ones calculated from empirical equations based on continuum mechanics.

To quantitatively describe the relationship between the unit cross drag F_d^{cross} on the nanotube and the flow speed U, simulations were performed for a set of flow speeds $U = 0.125 - 1.0$ (23.75-190 m/s), with an interval of 0.125. The drag force is plotted in Figure 6, in which the best fit parabolic curve is also presented. The equation for the fitted curve is expressed as

$$F_d^{cross} = -16.35U^2 + 69.74U, \quad 0 \le U \le 1. \quad (12)$$

Table 1: Reduced Units for a water-nanotube system

Quantity	Symbol	Reduced Units	Characteristic Value (S.I. Units)
Length		1	$\sigma_{OO} = 3.166 \times 10^{-10} m$
Mass	m	1	$m_{H_2O} = 2.99 \times 10^{-26} kg$
Energy	E	1	$\varepsilon_{OO} = 1.08 \times 10^{-21} J$
Charge	q	1	$q_H = 6.78 \times 10^{-20} C$
Time	t	1	$t = \sqrt{m_{H_2O}\sigma_{OO}^2/\varepsilon_{OO}} = 1.67 \times 10^{-12} s$
Force	F	1	$F = \varepsilon_{OO}/\sigma_{OO} = 3.41 \times 10^{-12} N$
Speed	v	1	$v = \sqrt{\varepsilon_{OO}/m_{H_2O}} = 1.90 \times 10^2 m/s$

This relationship will be used later in the simulation of nanotube dynamics in simple shear flow.

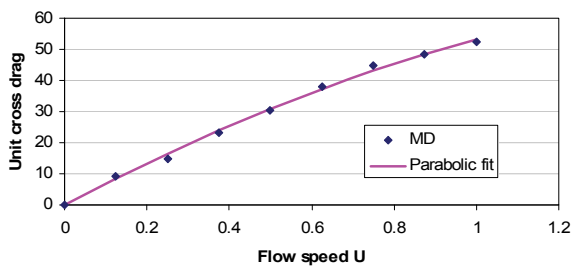

Figure 6: Unit cross drag on the nanotube in water flow as a function of the flow speed ($U = 0-1$, in reduced units)

3.4 Axial drag

The axial drag was obtained on a unit cell of $L \times W \times H = 7.96 \times 7.96 \times 0.85\, nm^3$, which contained 48 carbon atoms and 1776 water molecules. The simulation was performed in a similar way to the cross flow, except that the flow was in the longitudinal (z) direction of the nanotube and maintained by superimposing a desired flow velocity $\mathbf{U}$ on molecules within $0.025 \times L$ of the $x = \pm L/2$ boundaries and within $0.025 \times W$ of the $y = \pm W/2$ boundaries. The simulated axial drag is not sensitive to the increase in the domain size $L \times W$ or the domain thickness H. The simulated axial drag per unit length is plotted in Figure 7, where the best fit cubic curve is also presented. It is seen that the axial drag on the nanotube is very small in comparison with the cross drag. The equation for the fitted curve is expressed as

$$F_d^{axial} = 2.37\,U^3 + 6.07\,U^2 + 5.52\,U, \quad 0 \le U \le 1. \tag{13}$$

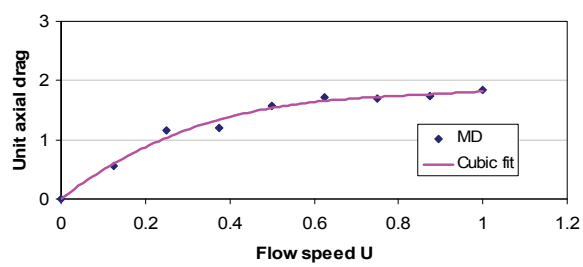

Figure 7: Unit axial drag on the nanotube in water flow as a function of the flow speed ($U = 0-1$, in reduced units)

3.5 End force

Above simulations show that the axial drag along the wall of an infinitely long nanotube (due to periodic boundary condition) is small. When a nanotube of finite length is placed in axial flow, the tube ends will also interact with fluid molecules. In this section, the force acting on the ends of a short nanotube in the axial flow is investigated. Figure 8 illustrates the unit cell of a short nanotube in an axial water flow system. In the $L \times W \times H$ three dimensional cell, an open-ended zigzag (6, 0) nanotube with a length of $l_{cnt} = 1.278\, nm$ was fixed at the center of the system. The initial state and boundary conditions were the same as in cross and axial flow. The flow was generated the same way as the cross flow but by

superimposing a desired flow velocity **U** in the z direction. Figure 9 shows the atomic structure of the nanotube. It consists of three repeating units which we call the left end (L_End), the middle part (M_Part), and the right end (R_End). In our simulation, the axial forces acting on the three parts were computed separately. When a domain size of $L \times W \times H = 4.66 \times 4.66 \times 6.21\,nm^3$ and a flow speed of $U = 1.0\,(190\,m/s)$ were used, the axial force on the middle part is about 0.26% of the force on the left end, both in the positive z direction, and the force on the right end is about 2.7% of the force on the left end but in the opposite direction. It can be concluded that when a nanotube is in axial flow, the axial force acting on the tube mainly comes from the left (upstream) end of the nanotube. The axial force on the left end, hereinafter referred to as the end force F_{end}, were investigated by changing the flow speed and the domain dimensions. Figure 10 plots the end force F_{end} as a function of flow speed U ($0 \le U \le 1$) for $L \times W \times H = 4.66 \times 4.66 \times 6.21\,nm^3$. Simulation results show that the end force is not sensitive to the increase in domain size. The equation for the best exponential fit is

$$F_{end} = 212.9\,U^{0.371}, \quad 0 \le U \le 1 \tag{14}$$

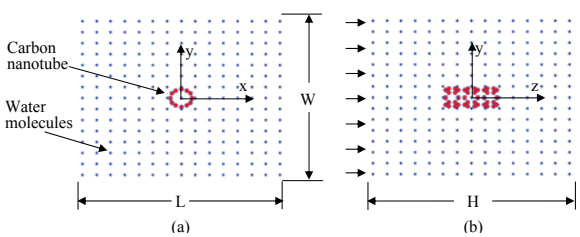

Figure 8: Unit cell of a short nanotube in axial water flow system: (a) top view; (b) side view

Figure 11 is a snapshot of the axial water flow around the nanotube. It should be noted that the water molecules did not enter the interior of the nanotube because the end openings are small.

4 Nanotube dynamics in simple shear flow

By coupling the drag forces on the nanotube with flexible fiber dynamics, the motion and deformation of a high aspect ratio carbon nanotube in simple shear flow can be simulated.

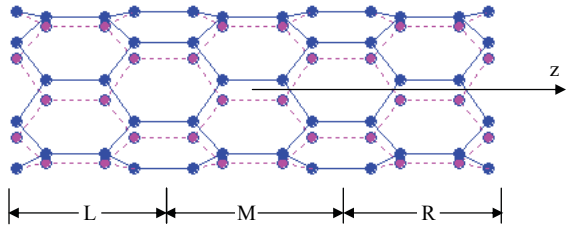

Figure 9: Atomic structure of the short zigzag (6, 0) nanotube

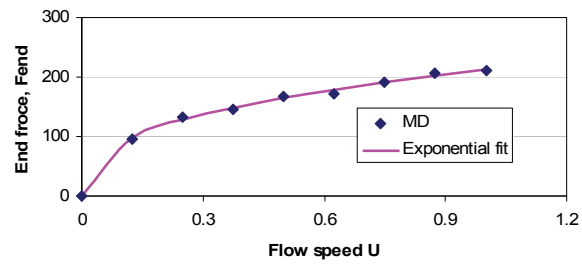

Figure 10: End force on the nanotube in water flow as a function of the flow speed ($U = 0-1$, in reduced units)

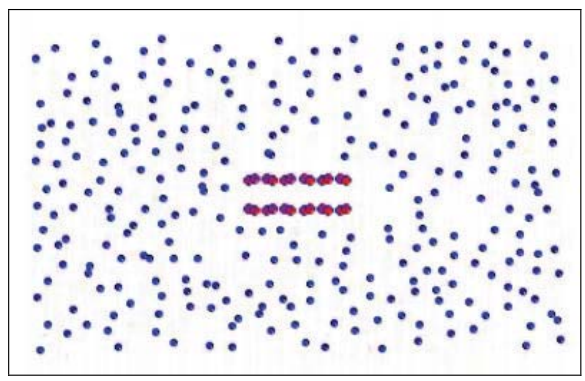

Figure 11: Snapshot of axial water flow around a short open-ended zigzag (6, 0) nanotube, illustrating no water molecules enter the tube interior

4.1 Case study of nanotube dynamics

Two cases of initially curved zigzag (6, 0) nanotube ($d = 0.4752\,nm$) as illustrated in Figure 12 are considered. Each nanotube consisted of two half-circles of radius equal to $4.752\,nm$. The aspect ratio (Ar) of the nanotubes was approxi-

mately 62.5. The flow field was defined as $u(y) = \dot{\gamma} \times y$, where $\dot{\gamma} = 0.001$ (reduced units) is the shear rate of the flow. We limited our calculations to two-dimensional flows, assuming that the nanotube motion and deformation only occur in the xy plane.

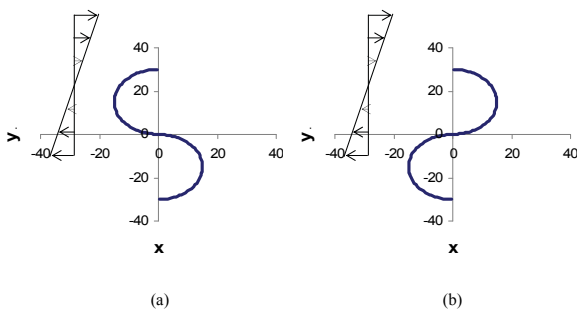

Figure 12: Initial configurations of two curved nanotubes: (a) s-shaped; (b) inverse-s shaped

A time step of $\Delta t = 0.02$ (reduced units) and a mesh size of $n = 17$ (number of discretized segments) were used in our calculations. Smaller steps and finer meshes do not change our simulation results. Figure 13 describes the configurations of the curved nanotubes at non-dimensional times t =0, 500, 1000, 2000, 4000 and 8000 respectively. Similar to macro scale curved fibers in simple shear flow, the curved nanotubes under shear become straight and align along the flow direction with time.

4.2 *Viscosity of a dilute nanotube-water suspension containing initially straight nanotubes oriented in the same direction*

The simulation of nanotube dynamics in flow allows us to investigate the effect of the presence of the nanotube on suspension viscosity. The viscosity of a dilute nanotube suspension was calculated using the same method for the dilute flexible fiber suspension. In this part, viscosity calculation will be performed on a single straight nanotube in simple shear water flow. Figure 14 illustrates a straight zigzag (6, 0) nanotube (Diameter: $d = 1.5008$ in reduced units; Aspect ratio:$Ar = 50$) initially placed in the middle of a unit cell with the tube axis normal to the shearing direction (flow shearing rate $\dot{\gamma} = 0.001$, reduced

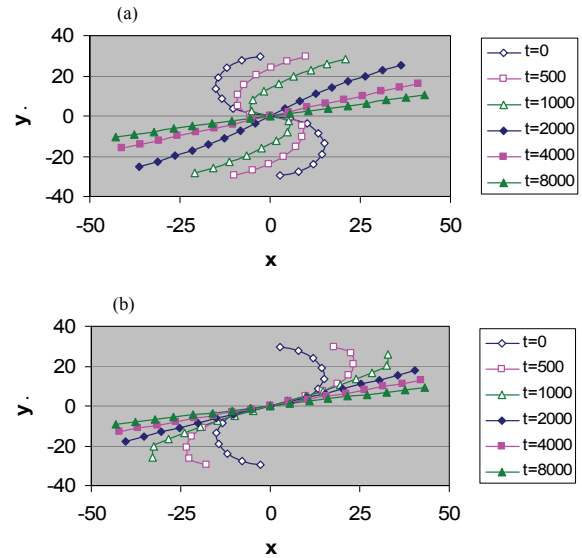

Figure 13: Motion of initially s-shaped and inverse-s-shaped nanotube in simple shear flow at different times (in reduced units)

units). The cell dimensions are $L \times W \times H = 100 \times 100 \times 30$(reduced units, cell thickness H in z direction is not presented in the figure). The volume fraction of the nanotube in the suspension is $V_f = 0.0442\%$. The unit cell is allowed to repeat itself in all the three directions. Thus the nanotubes in the dilute nanotube-water suspension are parallel to each other. Figure 15 illustrates the orientation of the nanotube at different times. In the shear flow field, the nanotube rotates and aligns along the shearing direction. Figure 16 plots the relative viscosity of the suspension as a function of the shear value $\dot{\gamma}t$. It is seen that the relative viscosity increases at the initial stage from unity to the maximum, which corresponds the tube orientation (about 45° to the shearing direction) at $t = 1000$ in Figure 15. As the orientation of the tube aligns along the flow direction, the relative viscosity approaches unity, or the suspension viscosity goes to the viscosity of the suspending fluid.

4.3 *Effect of nanotube aspect ratio on the suspension viscosity*

To investigate the effect of the aspect ratio of the nanotube on the viscosity of the suspension, four

Table 2: Dimensions of the unit cell of nanotube-water suspension containing an initially straight fiber (in reduced units)

Nanotube aspect ratio Ar	Tube length L_{cnt}	Cell length L	Cell width W	Cell thickness H
50	75.04	100	100	30
100	150.08	200	200	15
200	300.16	400	400	7.5
400	600.32	800	800	3.75

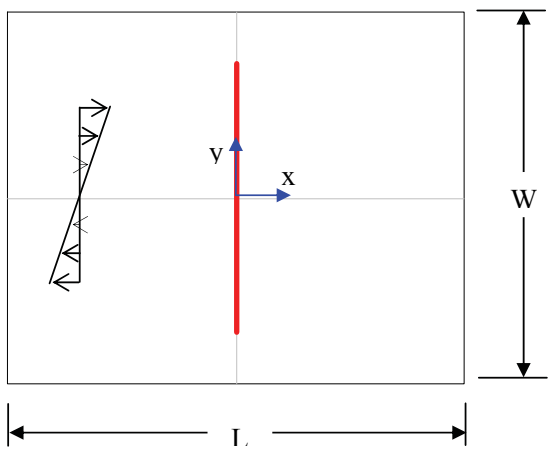

Figure 14: Unit cell of a nanotube-water suspension containing an initially straight nanotube

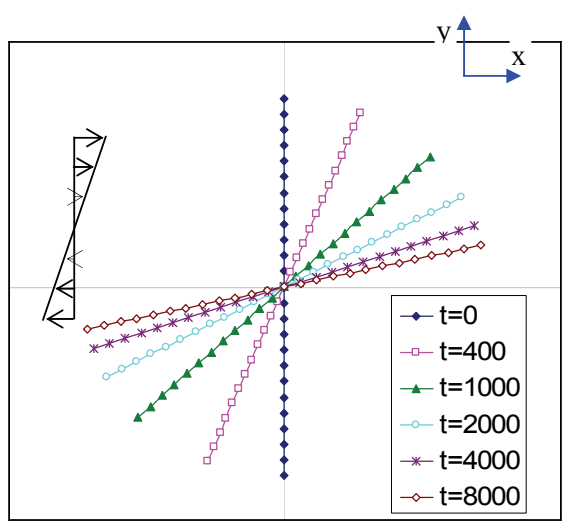

Figure 15: Rotation of an initially straight nanotube ($Ar = 50$) in shearing flow field ($\dot{\gamma} = 0.001$)

nanotubes of aspect ratios Ar =50, 100, 200 and 400 were simulated while the volume fraction of the nanotube in the suspension $V_f = 0.0442\%$ was

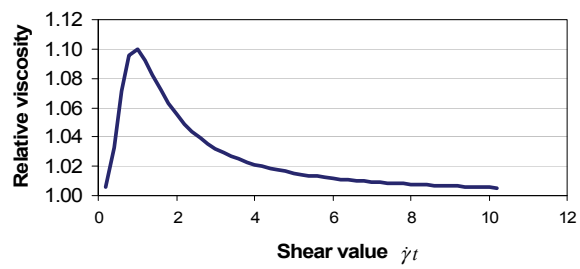

Figure 16: Relative viscosity of the nanotube-water suspension containing an initially straight nanotube ($Ar = 50$) as a function of the shear value $\dot{\gamma}t$ ($\dot{\gamma} = 0.001$)

kept constant. The cell dimensions $L \times W \times H$, which depend on the length of the nanotube, are listed in Table 2. Figure 17 presents the relative viscosity of the nanotube suspensions for the different nanotube aspect ratios. The maximum relative viscosity of the suspension as a function of the nanotube aspect ratio is plotted in Figure 18. It shows that at the same volume fraction, the suspension viscosity increases with the aspect ratio of the nanotube. This is because internal stresses in a longer nanotube can build up to a higher level than in a shorter tube, contributing to the larger increase in suspension viscosity.

4.4 *Effect of the nanotube volume fraction on the suspension viscosity*

For a dilute fiber suspension, the increase in the shear stress $\langle \tau_{xy} \rangle$ due to the presence of the fibers is linearly proportional to the volume fraction (V_f) of the fibers in the suspension (Equations 4). Since the bulk viscosity of the suspension is defined as the ratio of the shear stress to the shear rate, $\mu_{bulk} = \langle \tau_{xy} \rangle / \dot{\gamma}_{xy}$ (Equation 6), the increase in suspension viscosity μ_{bulk} due to the

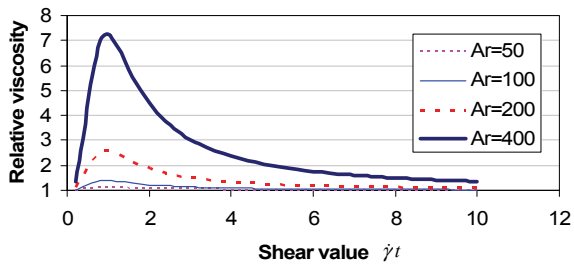

Figure 17: Relative viscosity of the nanotube-water suspensions as a function of the shear value $\dot{\gamma}t$ ($\dot{\gamma} = 0.001$). The suspensions contain an initially straight nanotube with the same nanotube volume fraction of $V_f = 0.0442\%$ but different nanotube aspect ratios (Ar =50, 100, 200 and 400)

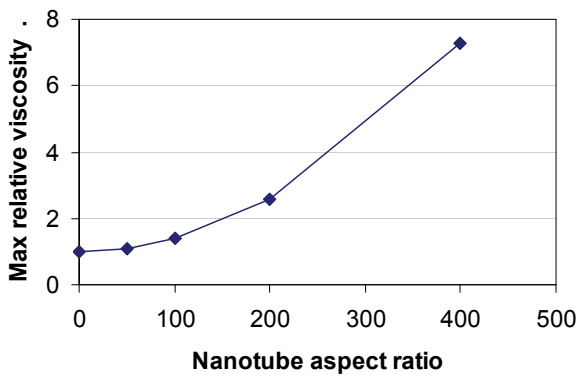

Figure 18: Maximum relative viscosity of the nanotube-water suspension as a function of the aspect ratio of the nanotube for $V_f = 0.0442\%$

fiber presence is also linearly proportional to the fiber volume fraction V_f. Based on the relative viscosity of the nanotube (Ar =400) suspension at $V_f = 0.0442\%$, the relative viscosity of the suspension for different nanotube volume fractions were calculated and plotted in Figure 19. It shows that when the nanotube volume fraction increases to $V_f = 0.708\%$, the maximum relative viscosity of the suspension is over 100, or the suspension viscosity is two orders higher than the fluid (water) viscosity. Table 3 presents qualitative comparison between our simulation and viscosity measurements by Kinloch et al. (2002) on nanotube-water suspensions with a cone and plate rheometer. In their measurements, at a shear rate $\dot{\gamma} = 1\,s^{-1}$ and a temperature of $T = 25°C$, the viscosity of a nanotube-water suspension for the nanotube volume fraction $V_f = 0.5\%$ is approximately 0.4 $Pa \cdot s$, about 450 times the water viscosity ($8.9 \times 10^{-4}\,Pa \cdot s$). It should be noted the parameters used in our calculation are different from those in Kinloch's measurements (Table 3).

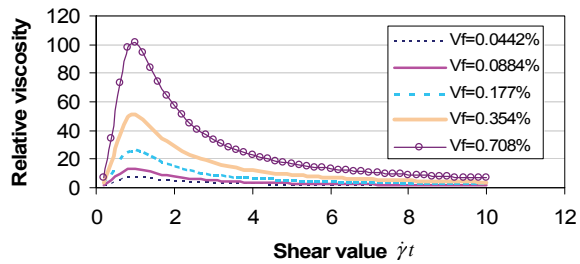

Figure 19: Relative viscosity of the nanotube-water suspension for different nanotube (Ar = 400) volume fractions

4.5 Effect of initial configuration of the nanotube on suspension viscosity

To investigate the effect of the initial configuration of the nanotube on the viscosity of nanotube suspension, three initial curvatures (straight, s-shaped and compact s-shaped) as illustrated in Figure 20 are considered. The three zigzag (6, 0) nanotubes with the same aspect ratio ($Ar = 62.5$) were used. The s-shaped nanotube is the same as the one used in the previous study on the dynamics of a curved nanotube in simple shear (Figure 12a). The compact s-shaped nanotube follows an elliptical contour. The shear flow field is the same as before ($\dot{\gamma} = 0.001$) and the nanotube volume fraction is 0.0276%. Figure 21 compares the relative viscosity of the nanotube suspension for different initial curvatures. It is seen that the suspension viscosity increases as the nanotube stretches from the compact s-shaped to the s-shaped and then to the straight configuration. This is because the difference in flow velocity over a more curved nanotube is smaller, resulting in a smaller difference in drag force over the tube which leads to lower internal forces and stresses in the nanotube. Therefore, the bulk stress is lower for the suspension containing a more curved nanotube, thus a lower suspension viscosity.

Table 3: Suspension parameters [Our simulation vs Kinloch's measurements (2002)]

	Our simulation	Kinloch's measurements
Type of nanotube	Single-walled	Multi-walled
Nanotube diameter d (nm)	0.4752	11 ± 3
Nanotube aspect ratio Ar	400	80 ± 48
Nanotube volume fraction V_f $(\%)$	0.708	0.5
Nanotube orientation	Parallel	Random
Relative viscosity of suspension	Maximum: ~ 102	$450 \sim 34$ $(\dot{\gamma} = 1 \sim 1000 s^{-1})$

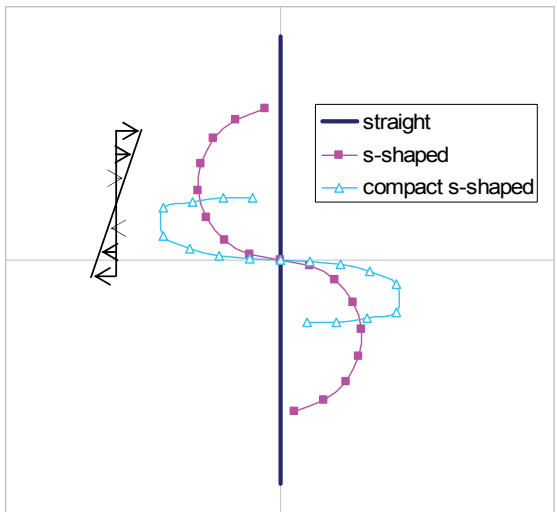

Figure 20: Role of initial nanotube configurations on suspension viscosity

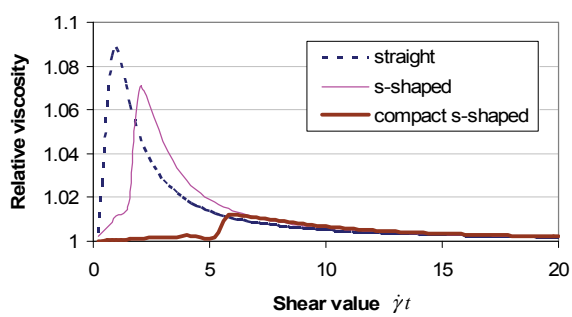

Figure 21: Comparison of suspension viscosity between different initial nanotube configurations but of same length (Ar =62.5)

4.6 *Viscosity of a dilute suspension containing uniformly oriented straight nanotubes representing an initial state of random orientation*

In the previous sections, the unit cells were assumed to repeat in all the three direction, resulting in a dilute nanotube-water suspension in which the nanotubes are parallel to each other. In this part, the suspension containing uniformly oriented nanotubes will be considered which represent a random orientation state with no preference in any particular direction. The unit cell of the suspension consists of 6 smaller sub-cells (a-f) in which the nanotubes take different initial orientations. The angles between the nanotubes to the shearing direction (x) are 0°, 30°, 60°, 90°, 120° and 150° respectively, with an angle interval of 30°.

Figure 22 shows the relative viscosity of the sub-cells and the whole suspension as a function of the shear value $\dot{\gamma}t$ when the following parameters were used: nanotube aspect ratio $Ar = 50$, nanotube volume fraction in each sub-cell $V_f = 0.0884\%$, and shear rate $\dot{\gamma} = 0.001$. The relative viscosity of the suspension was computed in a similar way to the viscosity calculation of the sub-cells (Equations 4 to 7) except that the bulk stress of the suspension was obtained by integrating over all the sub-cells. Figure 23 presents the relative viscosity of the suspension when the number of sub-cells is increased from 6 to 36. The angle intervals for 6, 12, 18 and 36 sub-cells are 30°, 15°, 10° and 5° respectively. It is seen that as the number of the sub-cells increases, the viscosity curve converges. Figure 24 shows the viscosity of the nanotube-water suspension containing evenly oriented straight nanotubes for aspect ratios of Ar =50, 100 and 200 respectively when 36 sub-cells are used. The nanotube volume fraction is $V_f = 0.884\%$ for all the three cases. The suspension viscosity increases with the aspect ratio of the nanotube. When the nanotube aspect ratio is $Ar = 200$, the maximum suspension viscosity is about 13.8 times the viscosity of the suspend-

ing water.

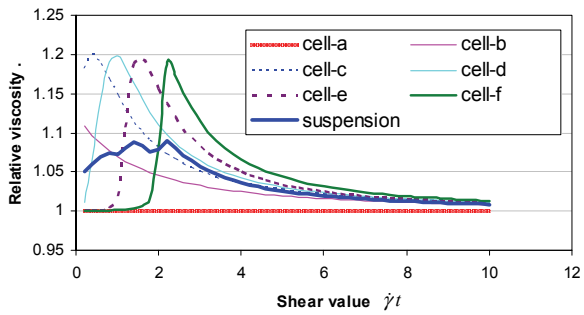

Figure 22: Viscosity of the dilute nanotube-water suspension containing 6 nanotubes with initial orientations of 0,30,60, 90, 120 and 150 ($Ar = 50$, 6 sub-cells)

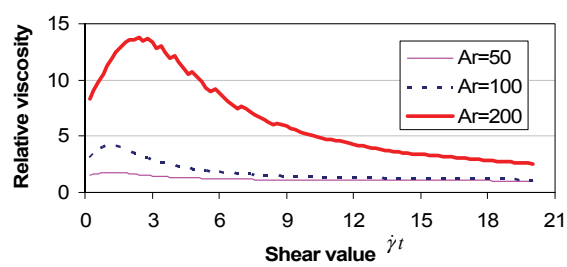

Figure 23: Viscosity of the dilute nanotube-water suspension containing increasing number of nanotubes (sub cells) with equally spaced initial orientations (Ar=50)

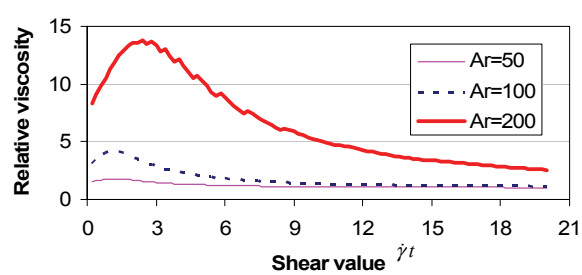

Figure 24: Viscosity of the dilute nanotube-water suspension initially containing uniformly oriented nanotubes for different nanotube aspect ratios using 36 sub-cells

5 Conclusions

In this work, a method for studying nanotube dynamics in simple shear flow was developed. The nanotube dynamics were investigated by coupling the flexible fiber dynamics with the drag forces on the nanotube obtained from MD simulations. It was shown that, like macro fibers, both initially s-shaped and inverse s-shaped nanotubes become straight and aligned along the shearing direction as time proceeds. The viscosity of a dilute nanotube-water suspension containing initially straight nanotubes oriented in the same direction was calculated based on nanotube dynamics. It was shown that the suspension viscosity increases with the aspect of the nanotube, since internal stresses can build up to a higher level in longer nanotubes which contribute to a larger increase in suspension viscosity. The increase in suspension viscosity due to the nanotube presence is proportional to the nanotube volume fraction V_f. It shows that, for the nanotube with an aspect ratio of $Ar = 400$, when the nanotube volume fraction increases to $V_f = 0.708\%$, the suspension viscosity is two orders higher than the viscosity of the suspending fluid, which is comparable to the published viscosity measurements on nanotube-water suspensions. Simulations also show that the viscosity of a nanotube suspension strongly depends on the curvature of the nanotube. In general, the difference in flow velocity over a more compacted nanotube is smaller than that over a more extended tube. Therefore the difference in drag force over a more compacted nanotube is smaller, translating into lower internal forces and stresses in the tube. Thus the bulk stress is lower for the suspension containing a more compacted nanotube, which leads to a lower suspension viscosity. The developed method can be used for dilute nanotube suspensions with random oriented nanotubes by employing a number subcells and using the assemblage averaging method to find the viscosity of the suspension.

Acknowledgement: This work was financially supported by the National Science Foundation on 'Processing of Nanotubes Using Liquid Composite Molding Techniques' under grant no. DMI-

0115127.

References

Abdel-Goad, M.; Potschke, P. (2005): Rheological characterization of melt processed polycarbonate-multiwalled carbon nanotube composites. *J. Non-Newtonian Fluid Mech*, vol. 128, pp. 2-6.

Advani, S.; Tucker, C. (1990): A numerical-simulation of short fiber orientation in compressing molding. *Polymer Composites*, vol. 11, pp. 164-173.

Ajayan, P.; Stephan, O.; Colliex, C.; Trauth, D. (1994): Aligned carbon nanotube arrays formed by cutting a polymer resin-nanotube composite. *Science*, vol. 265, pp. 1212-1214.

Ajayan, P.; Zhou, O. (2001): Applications of carbon nanotubes. *Carbon Nanotubes*, vol. 80, pp. 391-425.

Andrea, T., Swope, W.; Andersen, H. (1983): The role of long ranged forces in determining the structure and properties of liquid water. *J. chem. Phys,* vol. 79, pp. 4576-4584.

Bartus, S.D.; Vaidya, U.K. (2005): Performance of long fiber reinforced thermoplastics subjected to transverse intermediate velocity blunt object impact. *Composite structures*, vol. 67, pp. 263-277.

Batchelor, G.K. (1970): The stress system in a suspension of force-free particles. *J. Fluid Mech*, vol. 41, pp. 545-570.

Berendsen, H.; Grigera, J.; Straatsma, T. (1987): The missing term in effective pair potentials. *J. Phys. Chem,* vol. 91, pp. 6269-6271.

Bhattacharyya, A.; Sreekumar, T.; Liu, T.; Kumar, S.; Ericson, L.; Hauge, R.; Smalley, R. (2003): Crystallization and orientation studies in polypropylene/single wall carbon nanotube composite. *Polymer*, vol. 44, pp. 2373-2377.

Bojan, M.; Steele, W. (1987): Interactions of diatomic molecules with graphite. *Langmuir*, vol. 3, pp. 1123-1127.

Bretherton, F. (1962): The motion of rigid particles in a shear flow at low Reynolds number. *J. Fluid mech*, vol. 14, pp. 284-304.

Chiba, K.; Nakamura, K. (1998): Numerical solution of fiber suspension flow through a complex channel. *J. Non-Newtonian Fluid Mech*, vol. 78, pp. 167-185.

Dalmas, F.; Chazeau, L.; Gauthier, C.; Cavaille, J.; Dendievel, R. (2006): Large deformation mechanical behavior of flexible nanofiber filled polymer nanocomposites. *Polymer*, vol. 47, pp. 2802-2812.

Di Leo, J.; Maranon, J. (2003): Confined water in nanotube. *J. Molecular Structure-TheoChem*, vol. 623, pp. 159-166.

Du, F.; Fischer, J.; Winey, K. (2005): Effect of nanotube alignment on percolation conductivity in carbon nanotube/polymer composites. *Phys. Rev. B*, vol. 72, article no. 121404.

Falvo, M.; Clary, G.; Taylor, R.; Chi, V.; Brooks, F.; Washburn, S.; Superfine, R. (1997): Bending and buckling of carbon nanotubes under large strain. *Nature*, vol. 389, pp. 582-584.

Fan, Z.H.; Advani, S.G. (2007): Rheology of multiwall carbon nanotube suspensions. *J. Rheology*, Vol. 51, pp. 585-604.

Gordillo, M.C.; Marti, J. (2003): Water on the outside of carbon nanotube bundles. *Phys. Rev. B*, vol. 67, article no. 205425.

Hinch, E.J. (1976): The distortion of a flexible inextensible thread in a shearing flow. *J. Fluid Mech*, vol. 74, pp. 317-333.

Huang, Y.; Ahir, S.; Terentjev, E. (2006): Dispersion rheology of carbon nanotubes in a polymer matrix. *Phys. Rev. B*, vol. 73, article no. 125422.

Jeffrey, D.; Acrivos, A. (1976): Rheological properties of suspensions of rigid particles. *Aiche J.*, vol. 22, pp. 417-432.

Jeffery, G. (1923): The motion of ellipsoidal particles in a viscous fluid. *Proc. Royal Soc. London Series A*, vol. 102, pp. 161-179.

Joung, C.G.; Phan-Thien, N.; Fan, X.J. (2001): Direct simulation of flexible fibers. *J. Non-Newtonian Fluid Mech*, vol. 99, pp. 1-36.

Kalra, A.; Garde, S.; Hummer, G. (2003): Osmotic water transport through carbon nanotube membranes. *Proc. National Academy Sci. USA*,

vol. 100, pp. 10175-10180.

Kim J.; Lee, J.; Lee, D. (2005): Effect of fiber orientation on the tensile strength in fiber-reinforced polymeric composite materials. *Advances Fracture Strength*, vol. 297-300, pp. 2897-2902.

Kinloch, I.A.; Roberts, S.A.; Windle, A.H. (2002): A rheological study of concentrated aqueous nanotube dispersions. *Polymer*, vol. 43, pp. 7483-7491.

Kotsalis, E.M.; Walther, J.H.; Koumoutsakos, P. (2004): Multiphase water flow inside carbon nanotubes. *Inter. J. Multiphase Flow*, vol. 30, pp. 995-1010.

Kumar, S.; Doshi, H.; Srinivasarao, M.; Park, J.; Schiraldi, D. (2002): Fibers from polypropylene/nano carbon fiber composites. *Polymer*, vol. 43, pp. 1701-1703.

Kundu, P.K. (1990): *Fluid Mechanics*. Academic Press, California, USA.

Kusalik, P.G.; Svishchev, I.M. (1994): The spatial structure in liquid water. *Science*, vol. 265, pp. 1219-1221.

Liakus, J.; Wang, B.; Cipra, R.; Siegmund, T. (2003): Processing-microstructure-property predictions for short fiber reinforced composite structures based on a spray deposition process. *Composite Structures*, vol. 61, pp. 363-374.

Marion, J.B. (1970): Classical Dynamics of Particles and Systems. Academic Press, New York, USA: 197-200.

McClelland, A.N.; Gibson, A.G. (1990): Rheology and fibre orientation in the injection moulding of long fibre reinforced nylon 66 composites. *Composites manufacturing*, vol. 1, pp. 15-25.

Rapaport, D.C. (1995): *The Art of Molecuar Dynamics Simulation*. Cambridge University Press, New York, USA.

Ross, R.F.; Klingenberg, D.J. (1997): Dynamic simulation of flexible fibers composed of linked rigid bodies. *J. Chem. Phys*, vol. 106, pp. 2949-2960.

Ruoff, R.; Lorents, D. (1995): Mechanical and thermal properties of carbon nanotubes. *Carbon*, vol. 33, pp. 925-930.

Sung, Y.; Han, M.; Song, K.; Jung, J.; Lee, H.; Kum, C.; Joo, J.; Kim, W. (2006): Rheological and electrical properties of polycarbonate/multi-walled carbon nanotube composites. *Polymer*, vol. 47, pp. 4434-4439.

Tang, W.; Advani, S.G. (2005): Dynamic simulation of long flexible fibers in shear flow. *CMES: Computer Modelling in Engineering & Sciences*, vol. 8, pp. 165-176.

Tang, W.; Advani, S.G. (2006): Drag on a nanotube in uniform liquid argon flow. *J. Chem. Phys*, vol. 125, article no. 174706.

Tang, W.; Advani, S.G. (2007): Non-Equilibrium Molecular Dynamics Simulation of Water Flow around a Carbon Nanotube. *CMES: Computer Modelling in Engineering & Sciences*, vol. 22, pp. 31-40.

Taylor, G. (1923): The motion of ellipsoidal particles in a viscous fluid. *Proc. Royal soc. London Series A*, vol. 103, pp. 58-61.

Thostenson, E.; Chou, T. (2002): Aligned multi-walled carbon nanotube-reinforced composites: processing and mechanical characterization. *J. Phys. D -Appl. Phys*, vol. 35, pp. L77-L80.

Timoshenko, S.P.; Goodier, J.N. (1970): Theory of Elasticity. McGRAW-Hill, Singapore: 17-19.

Tornberg, A.K.; Shelley, M.J. (2004): Simulating the dynamics and interactions of flexible fibers in Stokes flows. *J. Computational Phys*, vol. 196, pp. 8-40.

Trevelyan B.; Mason, S. (1951): Particle motions in sheared suspensions: 1 rotations. *J. Colloid Sci*, vol. 6, pp. 354-367.

Walther, J.H.; Werder, T.; Jaffe, R.L.; Koumoutsakos, P. (2004): Hydrodynamic properties of carbon nanotubes. *Phys. Rev. E*, vol. 69, article no. 062201.

Werder, T.; Walther, J.H.; Jaffe, R.L.; Halicioglu, T.; Koumoutsakos, P. (2003): On the water-carbon interaction for use in molecular dynamics simulations of graphite and carbon nanotubes. *J. Phys. Chem. B*, vol. 107, pp. 1345-1352.

Yamamoto, S.; Matsuoka, T. (1993): A method for dynamic simulation of rigid and flexible fibers

in a flow field. *J. Chem. Phys*, vol. 98, pp. 644-650.

Yamamoto, S.; Matsuoka, T. (1994): Viscosity of dilute suspension of rodlike particles: A numerical simulation method. *J. Chem. Phys*, vol. 100, pp. 3317-3324.

Vincent, M.; Agassant, J. (1985): Experimental and theoretical study of short fiber orientation in diverging flows. *RHEOLOGICA ACTA*, vol. 24, pp. 603-610.

Xu H.; Aidun, C. (2005): Characteristics of fiber suspension flow in a rectangular channel. *Inter. J. Multiphase Flow*, vol. 31, pp. 318-336.